J Sol-Gel Sci Technol (2015) 74:513–520
DOI 10.1007/s10971-015-3627-2

ORIGINAL PAPER

Structural characterization of N-doped anatase–rutile mixed phase TiO_2 nanorods assembled microspheres synthesized by simple sol–gel method

M. A. Mohamed · W. N. W. Salleh · J. Jaafar · A. F. Ismail

Received: 23 October 2014 / Accepted: 10 January 2015 / Published online: 23 January 2015

Abstract In this study, N-doped anatase–rutile mixed phase TiO_2 nanorods assembled microspheres were synthesized via a direct and simple sol–gel method. The physical analysis via X-ray diffraction indicated that the prepared sample had a mixed phase of anatase and rutile TiO_2. The morphology of the structure was observed with field emission scanning electron microscopy, transmission electron microscopy and atomic force microscopy, which showed that the formation of TiO_2 microspheres was constructed by TiO_2 nanorods or rice like structure nanorods. Besides, Fourier transform infrared analysis revealed that the presence of $N_2O_2^{2-}$ and NO^- species in the spectra while XPS study indicated the incorporation of nitrogen as dopant in TiO_2 at binding energies of 396.8, 397.5, 398.7, and 399.8 eV. Furthermore, the optical properties determined by UV–Vis spectroscopy concluded that the prepared sample exhibited excellent optical responses to UV and visible region as well as being a potential material for degradation of hazardous water pollutants. The photocatalytic activity of the prepared TiO_2 exhibits excellent photodegradation of methylene blue under UV and visible light irradiation.

Graphical Abstract

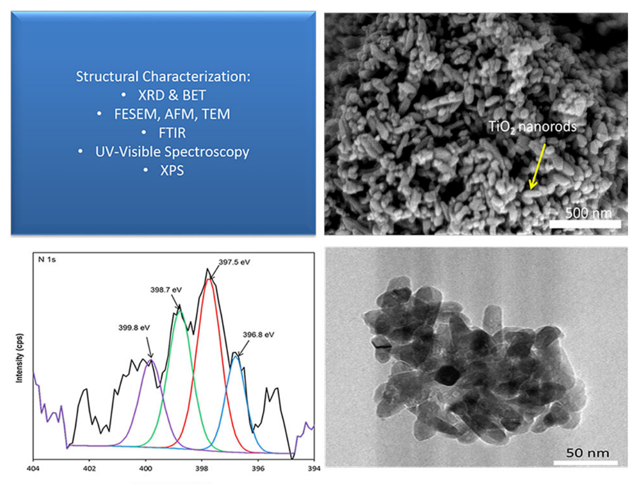

Keywords N-doped TiO_2 nanorods · Anatase/Rutile · UV–visible irradiation · Sol–gel preparation · Structural characterization

1 Introduction

Titanium dioxide (TiO_2) is one of the semiconductors that have been widely used as a photocatalyst in water and wastewater treatment due to its chemical stability, low cost, excellent optical and electronic properties, as well as high photocatalytic activity [1, 2]. Compared to rutile and brookite, anatase had shown the highest photocatalytic activity in the degradation of various organic pollutants in wastewater treatment. Most of the previous studies have focused on the preparation of single-phase TiO_2 nanostructures [1–5]. In

M. A. Mohamed · W. N. W. Salleh · J. Jaafar · A. F. Ismail
Advanced Membrane Technology Research Centre, Universiti Teknologi Malaysia (UTM), 81310 Johor Bahru, Johor, Malaysia

M. A. Mohamed · W. N. W. Salleh (✉) · J. Jaafar · A. F. Ismail
Faculty of Petroleum and Renewable Energy Engineering, Universiti Teknologi Malaysia (UTM), 81310 Johor Bahru, Johor, Malaysia
e-mail: hayati@petroleum.utm.my

addition, a recent study revealed that the combination of anatase–rutile mixed phase exhibited excellent photocatalytic activity compared to its single constituents [6–10]. The excellent photocatalytic activity is due to the synergy effect between anatase and rutile, which promotes interfacial electron transfer from rutile to anatase [7].

Recently, many studies have been conducted to improve the photoabsorption features of TiO_2 under UV and visible light irradiation [11, 12]. However, to the best of our knowledge, there is hardly a report on the preparation of nitrogen doped anatase–rutile mixed phase TiO_2 nanostructures [13, 14]. Therefore, it would be interesting to prepare doped anatase–rutile mixed-phase TiO_2 nanostructure with high photocatalytic activity under UV and visible light irradiation. The substitution with nitrogen doping in TiO_2 lattice structure is particularly effective to narrow the band gap of TiO_2, as well as to provide high photocatalytic activity under visible light irradiation [11].

Thus, in this study, N-doped anatase–rutile mixed phase TiO_2 nanorods assembled microspheres with broad range UV and visible light absorbing capacity was prepared via a direct and simple sol–gel method. The crystallinity, morphology, structural analysis, and optical properties of the produced N-doped anatase–rutile mixed-phase TiO_2 nanorods assembled microspheres had been characterized.

2 Experimental method

2.1 Materials

All the chemicals used were of analytical reagent grade and were used as received. Titanium-n-butoxide $Ti(OBu)_4$ from Sigma-Aldrich was used as a titanium precursor. Nitric acid (HNO_3) 65 % and isopropanol (C_3H_7OH) were obtained from QReC Chemicals. Isopropanol and distilled water were used as the dispersing media.

2.2 Method

N-doped Anatase/Rutile Mixed Phase TiO_2 was synthesized through acid modified sol–gel method. At room temperature, 25 mL of $Ti(OBu)_4$ was dissolved in 8 mL of isopropanol under constant magnetic stirring. The mixture was added dropwise into 200 mL of distilled water under vigorous stirring for 30 min. Then 3 mL of 65 % of HNO_3 was added dropwise into the mixture under vigorous stirring for about 60 min. Subsequently, the obtained sol was aged in tight air for 3 days or more at room temperature until gel formation took place. The resultant gel was then dried at 75 °C for 3 days in a vacuum oven until a yellowish solid was obtained and denoted as T75. The obtained solid was ground and calcined at 400 °C for 2 h and denoted as T400.

2.3 Characterization

2.3.1 *X-ray diffraction and BET surface area*

An X-ray diffraction (XRD) analysis was carried out to study the crystallinity and the phase formation of the sample using an X-ray diffractometer (SIEMENS XRD D5000). The measurements were carried out at 40 kV and 40 mA, which employed a CuKα radiation at a wavelength of 0.15418 nm at an angular incidence of $2\theta = 20–80°$. The BET surface area was measured by nitrogen adsorption–desorption analysis.

2.3.2 *Morphological analysis*

A morphological study of the sample was carried out using FESEM (HITACHI) at an accelerated voltage of 2.0 kV. Transmission electron microscopy (TEM) was conducted using EFTEM LIBRA-120, Carl Zeiss AG Company (Oberkochen, Germany). The AFM measurement was performed using (XE-100 Park System) an atomic force microscope with SSS-NCHR non-contact probes at 1 μm/s of scan speed.

2.3.3 *Fourier transform infrared spectroscopy*

An investigation on the presence of N-dopant in the sample was performed with Perkin Elmer FT-IR ATR spectrophotometer and diamond ATR sampling accessory. The spectrum of the sample was scanned with the wavenumber ranging from 4,000 to 650 cm^{-1}.

2.3.4 *UV–visible spectroscopy*

The optical property of the prepared sample was evaluated with UV–Vis–NIR spectrophotometer (UV-3101PC Shidmadzu) between 200 and 600 nm.

2.3.5 *X-ray photoelectron spectroscopy (XPS)*

The X-ray photoelectron spectroscopy (XPS) spectra of the prepared sample were attained by means of Kratos Analytical Axis Ultra DLD photoelectron spectrometer using AlKα radiation monochromatic source.

2.4 Photocatalytic activity measurement

In order to evaluate the photocatalytic activity of the prepared N-doped TiO_2, methylene blue was used as model water pollutants under UV and visible light irradiation. The prepared N-doped TiO_2 (0.15 g) was added in an aqueous solution containing 150 mL of methylene blue with a concentration of 30 mg/L. The suspension was sonicated for 15 min and stirred in dark place for 30 min to reach adsorption–desorption equilibrium. The suspension was irradiated using ultraviolet (UV) lamp (Vilber Laurmat, λ = 312 nm, 30 W) and white light-emitting diode (LED) flood light (CS-FL-30 W, λ > 420 nm, 30 W) manufactured by Wuhan Co-Shine Technology Co., Ltd. China. Before analysis, the suspension (3 mL) was taken through a syringe filter and treated as initial concentration (C_0). Subsequently, the lamp was turned on and the suspension was collected at regular time intervals during irradiation and filtered through syringe filter. The differential absorbance at 664 nm for methylene blue (absorption peak methylene blue) was measured. The change in the concentration of methylene blue of the irradiated sample with time was monitored by Perkin Elmer UV–Visible spectrophotometer and compared with the blank (photolysis of methylene blue under UV and visible light irradiation without the presence of photocatalyst) carried out at the same experimental conditions. The photocatalytic behavior of the Degussa P25 and pure anatase supplied by Sigma-Aldrich was also measured for comparison study.

3 Result and discussion

3.1 X-ray diffraction and BET Surface Area

The XRD patterns of the N-doped Anatase/Rutile Mixed Phase TiO_2 nanorod are shown in Fig. 1. It can be seen that the main diffraction peak of anatase (101) and rutile (110) were observed at $2\theta = 25.4°$ and $2\theta = 27.5°$. Besides, small traces of diffraction peak signals of the brookite phase were observed in the sample at $2\theta = 30.85°$. The weight fraction (WR) between anatase and rutile was calculated by using the following equation:

$$WR = \frac{\mathrm{Ar}}{0.884Aa + \mathrm{Ar}} \quad (1)$$

where Ar represents the intergrated intensity of the rutile (110) peak, and Aa is the intergrated intensity of the anatase (101) peak [15], which had been found to be 39 % anatase and 61 % rutile. The average sizes of crystallite for anatase and rutile in each sample were estimated using the Scherrer equation [16], and it had been discovered that the average sizes of crystallites for anatase and rutile were 9 and 30 nm respectively, and 20 nm in average. The specific surface area of the prepared TiO_2 was determined by N_2 adsorption–desorption isotherms. The results showed that the BET specific surface area of the prepared TiO_2 (73 $m^2\ g^{-1}$) was higher than P25 (52 $m^2\ g^{-1}$) and pure anatase (15 $m^2\ g^{-1}$). It is indicated that the prepared TiO_2 had smaller crystallite size as compared to P25 and pure anatase, which promote more catalytic active surface sites per unit catalyst mass.

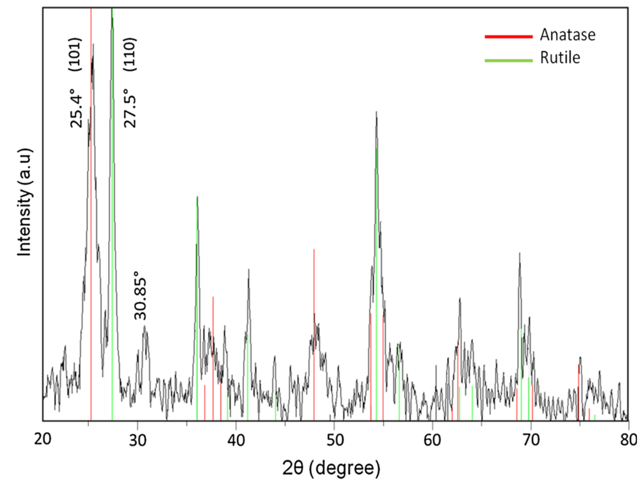

Fig. 1 XRD pattern of N-doped anatase/rutile mixed phase TiO_2 nanorod calcined at 400 °C

3.2 Morphological analysis

The morphological structure of the prepared TiO_2 was investigated using FESEM, TEM, and AFM. Both images taken from FESEM and AFM showed that TiO_2 microspheres are constituted by assembled TiO_2 nanorods or rice like structures, as shown in Fig. 2. A similar result has been reported by Ruan and coworkers [13]. Based on the AFM images (see Fig. 2c, d, the size of TiO_2 nanorod was roughly estimated to be below than 50 nm. The single formation of TiO_2 microspheres assembled by TiO_2 nanorods can also be observed by TEM image as shown in Fig. 3. It is confirmed that the formation of this microsphere was constructed by TiO_2 nanorods with an average length of 70 nm and average width of 16 nm. These results were consistent with the XRD results presented in the Sect. 3.1.

3.3 FTIR spectroscopic analysis

Figure 4 shows the FTIR spectra of the synthesized N-doped anatase/rutile mixed phase TiO_2 nanorods prepared at 400 °C in the wavenumber range of 650–4,000 cm^{-1}. It was observed that all spectra exhibited two dominant absorption regions found at 3,000–3,200 cm^{-1} and at 1,000–1,700 cm^{-1}. The broad peak located at 3,100 cm^{-1} is due to the stretching of –OH groups. A relatively sharp peak observed at 1,625 cm^{-1} is associated to –OH bending mode of water on the surface of the TiO_2 [2]. Meanwhile, the absorption at 1,396 cm^{-1} is due to –C–H stretching vibration peaks corresponding to the presence of organic species contaminant on the surface from alkoxide precursor [2, 17, 18]. Moreover, the obvious peaks around 1,346 and 1,095 cm^{-1} in samples T75 and T400 are due to the presence of $N_2O_2^{2-}$ and NO^- species [17, 19]. The presence of these two peaks indicate that $N_2O_2^{2-}$ and

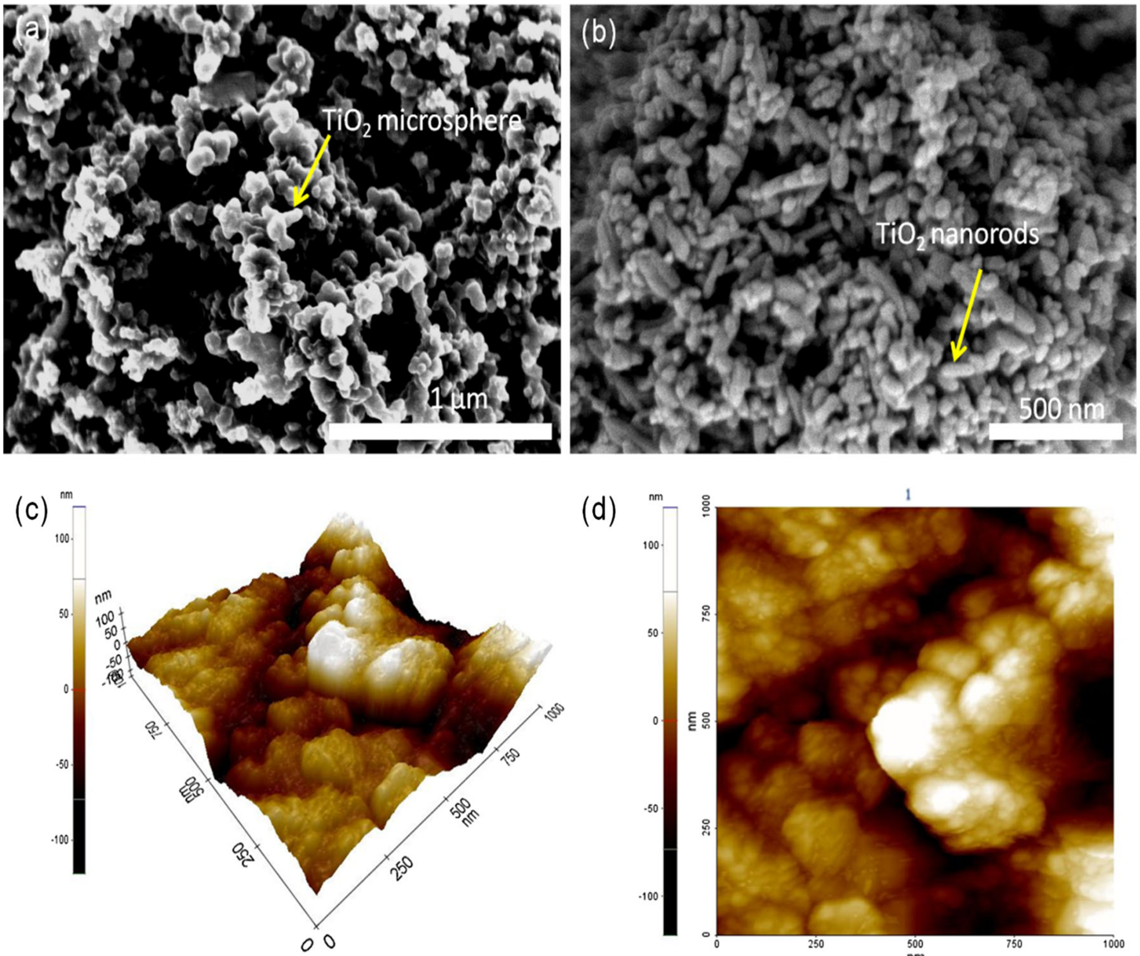

Fig. 2 FESEM micrographs of N-doped anatase/rutile mixed phase TiO_2 nanorod calcined at 400 °C: **a** low magnification, **b** high magnification; AFM images, **c** 3D view, and **d** height view

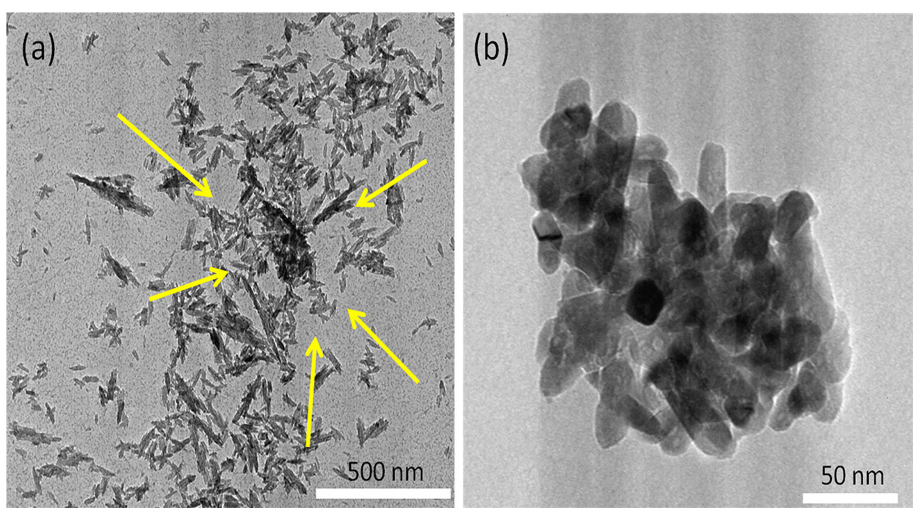

Fig. 3 TEM image of the TiO_2 microsphere assembled TiO_2 nanorods

NO^- species could be chemisorbed on the surface of the synthesized TiO_2 and not affected as they had undergone calcination processes up to 400 °C. In the present study, almost all the prepared TiO_2 samples were activated in the visible light, which might be ascribed to the *N* doping during the preparation process using HNO_3 [20].

3.4 UV–Visible spectroscopy

The optical response of the prepared TiO_2 was investigated by means of UV–Vis absorption spectra, as shown in Fig. 5. The prepared TiO_2 exhibited excellent optical responses to UV and visible region. The introduction of nitrogen in the TiO_2 lattice structure led to the capability to absorb higher fraction of photons from the visible region [21, 22]. Furthermore, compared to the previous study, the uses of HNO_3 as nitrogen doping sources significantly improved the absorbance under visible irradiation [11]. The same finding can also be found in a study conducted by Zhang et al. [17].

3.5 X-ray photoelectron spectroscopy (XPS)

The concentration and the electronic state of the nitrogen on the surface of the prepared TiO_2 were measured by XPS. As shown in Fig. 6, it is revealed that the surface of the prepared TiO_2 was composed of Ti, O, N, and C contaminants. The C 1s spectra of the prepared TiO_2 are shown in Fig. 7. The peaks of the binding energies corresponding to C 1s are observed at 283.1, 284.4, 286.8, and 288.2 eV, which can be assigned to C, C–C or C–H, C–O, and C = O [17, 23]. These peaks can be assigned to adventitious carbon contamination species from XPS measurement [18, 24]. Recent study reported by Xing et al. [25] have suggested that the peak at 283.1 eV can be ascribed to interstitial carbon species in TiO_2 to form Ti–O–C bonds. The concentration of C in the TiO_2 lattice is about 31.3 % (atomic percent) which is relatively higher than reported by previous study (0.19–0.28 %) [18]. Dong et al. [18] reported that the low concentration of C doped in the prepared TiO_2 enhanced the visible light absorption

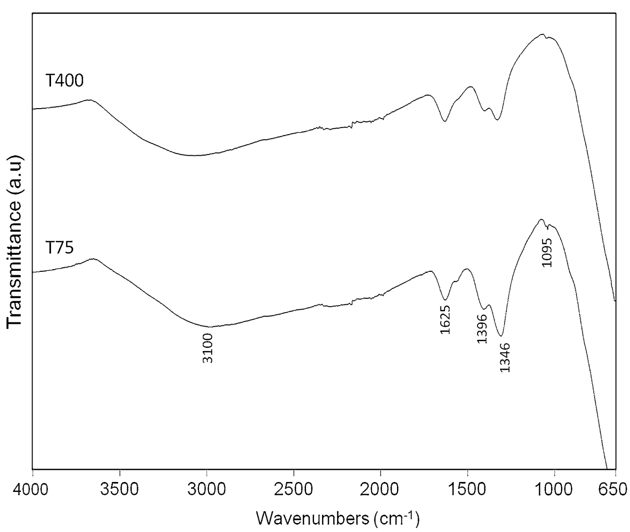

Fig. 4 FTIR spectra of T75 and T400

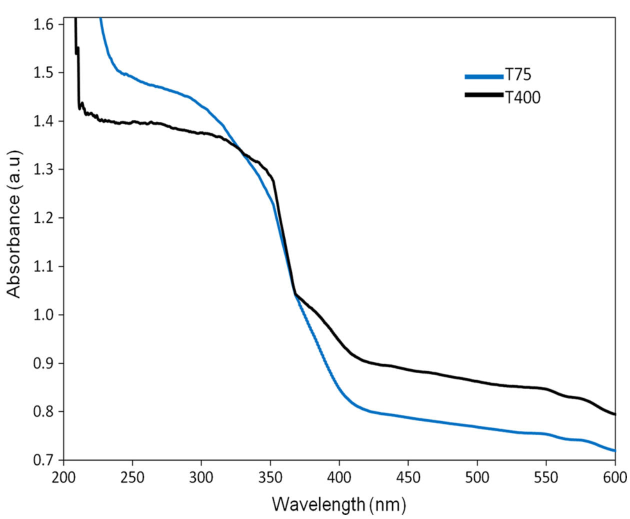

Fig. 5 UV–visible absorption spectrum of T75 and T400

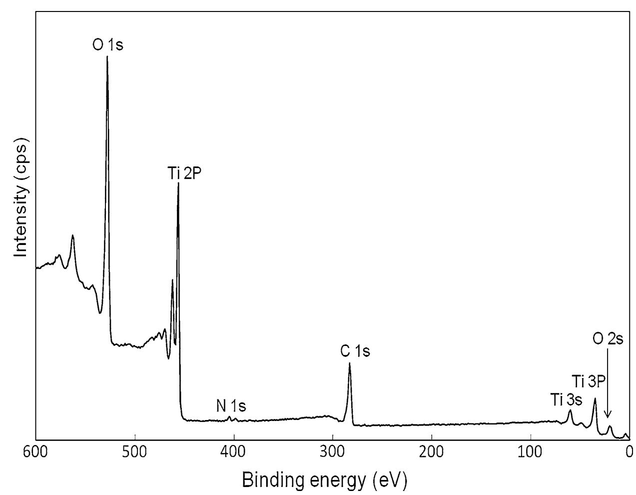

Fig. 6 XPS survey spectra of T400 sample

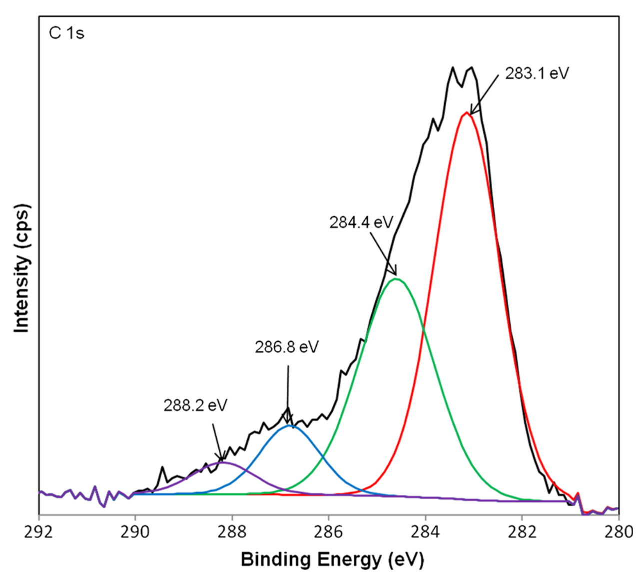

Fig. 7 XPS spectra of C 1s peak of T400 sample

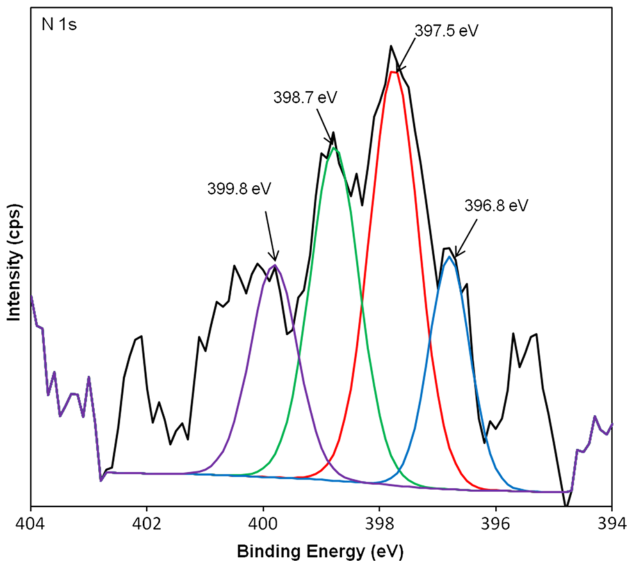

Fig. 8 XPS spectra of N 1s peak of T400 sample

capability. They also observed that the C 1s peaks at 282.3 and 282.5 eV was attributed to O–Ti–C bond. Furthermore, previous studies suggested that the carbon substituting for oxygen atom in TiO_2 lattice structure which related to the visible light responsibility was commonly observed at peak 281–282 eV resulting from Ti–C bonds [17, 26–28]. Thus, the Ti–O–C bond might be not favourable to the visible light absorption capability as compared to Ti–C and O–Ti–C bonds. It is noteworthy that XPS results clearly ruled out the existence of C as a dopant in the N–TiO_2 photocatalysts because the doped carbon in TiO_2 exhibits a very low C 1s binding energy at 281–282 eV [29].

The range of the binding energy from 404 to 394 eV corresponds to the peak of N 1s are shown in Fig. 8. The binding energies of N 1s for sample T400 was detected at 396.8, 397.5, 398.7, and 399.8 eV. Previous studies suggested that the N 1s peak of the N-doped TiO_2 was commonly observed between 395 and 402 eV [15, 17, 30–34]. The existence of the binding energy at 396.8, 397.5, 398.7, and 399.8 eV has confirmed the success of the N-doping in the TiO_2 lattice structure. The peak at 396.8 eV is attributed to the Ti–N bonds in TiO_2 [35]. Previous studies reported that the binding energy at 397.5 eV is indicative of N atom replacing oxygen in the TiO_2 crystal lattice and the formation of N–Ti–N bond [36–39]. The N 1s peak of the prepared TiO_2 at 399.8 eV can be attributed to interstitial nitrogen species or the presence of oxidized nitrogen similar to NO*x* species which the possibility of N–O–Ti or Ti–N–O bond formed on the TiO_2 crystal surface [40–42]. From XPS analysis, the concentration of the nitrogen in the TiO_2 crystal lattice is about 1.5 % (atomic percent). At lower doping levels ($\leq$2.1 % atomic percent), previous studies concluded that the substitutional N atom in TiO_2 crystal lattice will introduce localized N 2p states above the valence band which improves the absorption capability under visible light irradiation [43]. The results showed that the concentration of the nitrogen in the prepared sample is varied as compared to the previous study. It is might be due to the sample preparation techniques and nitrogen sources [17, 22, 36, 44].

3.6 Photocatalytic activity measurement

The photodegradation of the methylene blue has been conducted to evaluate the photocatalytic activity of the prepared TiO_2 under UV and visible light irradiation. Figure 9a, b illustrate the photodegradation curves of methylene blue under UV and visible light irradiation conducted for 360 and

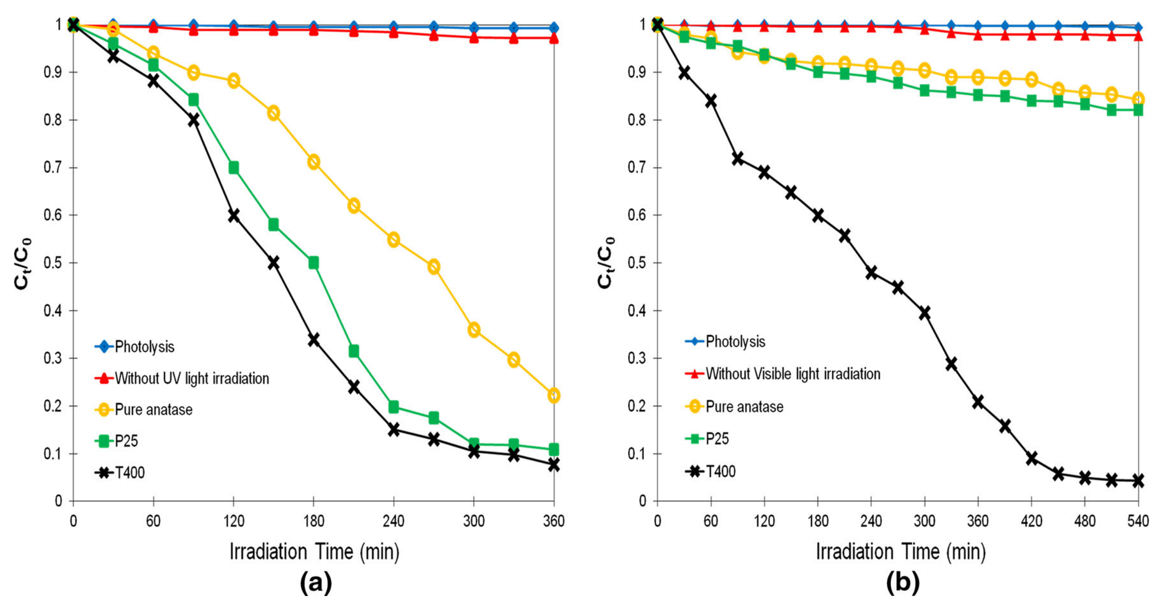

Fig. 9 Photodegradation of methylene blue under **a** UV light irradiation and **b** visible light irradiation

540 min, respectively. It is indicated that the prepared TiO_2 had photocatalytic activity under UV and visible light irradiation with degradation percent of 92.2 and 95.7 %, respectively. The photolysis study proved that the methylene blue is stable under UV and visible light irradiation. In addition, the reduction in the concentration of the methylene blue without UV and visible light irradiation were very low with degradation percent of 2.2 and 2.8 %, respectively. These results generally show that the system has reached the adsorption–desorption equilibrium. It is indicated that the photodegradation of the methylene blue can occur only with the present of photocatalyst and light irradiation. The prepared TiO_2 (T400) was active under UV and visible light irradiation while P25 and pure anatase only active under UV light irradiation. It can be seen in Fig. 7b that, both P25 and pure anatase exhibit very low photocatalytic activity with degradation percent of 17.9 and 15.7 %, respectively. The prepared TiO_2 (T400) exhibit excellent photocatalytic degradation of methylene blue under visible light irradiation. It is due to the present of nitrogen atom in TiO_2 lattice structure. The nitrogen doping in the TiO_2 lattice structure could enhance the absorption capability in visible light irradiation [34, 36, 44–47].

4 Conclusion

The N-doped anatase/rutile mixed phase TiO_2 nanorod assembled microspheres were successfully synthesized by simple sol–gel method. The formation of TiO_2 nanorod assembled microsphere was confirmed via FESEM, TEM, and AFM. The size of TiO_2 produced was found to be <50 nm with relatively high degree of crystallinity in anatase/rutile mixed phase. The formation of anatase/rutile mixed phase, assisted by calcinations temperature at 400 °C, is believed to improve the photocatalytic activity attributed to the electron affinity within the anatase and rutile phases. The substitution doping with nitrogen in the TiO_2 lattice structure was confirmed by XPS analysis. The results proved that the resultant TiO_2 exhibited good optical properties as it could absorb both UV and visible light irradiation suit for a broad range of application for the elimination of organic pollutants in wastewaters.

Acknowledgments The authors acknowledge the support from Ministry of Higher Education Malaysia (Research University Grant Scheme (GUP)) (Vot No. 05H08) and Universiti Teknologi Malaysia (UTM) for funding this research project.

References

1. Liu M, Piao L, Zhao L et al (2010) Anatase TiO_2 single crystals with exposed 001 and 110 facets: facile synthesis and enhanced photocatalysis. Chem Commun (Camb) 46:1664–1666. doi:10.1039/b924172h
2. Li S, Ye G, Chen G (2009) Low-temperature preparation and characterization of nanocrystalline anatase TiO_2. J Phys Chem C 113:4031–4037
3. Li Z, Liu R, Xu Y (2013) Larger effect of sintering temperature than particle size on the photocatalytic activity of anatase TiO_2. J Phys Chem C 117:24360–24367
4. Ao Y, Xu J, Fu D et al (2008) Low temperature preparation of anatase TiO_2^- coated activated carbon. Colloids Surf A Physicochem Eng Asp 312:125–130. doi:10.1016/j.colsurfa.2007.06.039
5. Liu X (2012) Preparation and characterization of pure anatase nanocrystals by sol–gel method. Powder Technol 224:287–290. doi:10.1016/j.powtec.2012.03.007
6. Scanlon DO, Dunnill CW, Buckeridge J et al (2013) Band alignment of rutile and anatase TiO_2. Nat Mater 12:798–801. doi:10.1038/nmat3697
7. Apopei P, Catrinescu C, Teodosiu C, Royer S (2014) Mixed-phase TiO_2 photocatalysts: crystalline phase isolation and reconstruction, characterization and photocatalytic activity in the oxidation of 4-chlorophenol from aqueous effluents. Appl Catal B Environ 160–161:374–382. doi:10.1016/j.apcatb.2014.05.030
8. Zhang Y, Chen J, Li X (2010) Preparation and photocatalytic performance of anatase/rutile mixed-phase TiO_2 nanotubes. Catal Lett 139:129–133. doi:10.1007/s10562-010-0425-x
9. Kalashnikova A, Nikolenko N, Kalashnikov J, Kostynyuk A (2013) Rutile–anatase composite catalyst formed by coupling anatase and rutile particles. Chem Mater Eng 1:88–95. doi:10.13189/cme.2013.010305
10. Xiong Z, Wu H, Zhang L et al (2014) Synthesis of TiO_2 with controllable ratio of anatase to rutile. J Mater Chem A 2:9291. doi:10.1039/c4ta01144a
11. Ruzimuradov O, Nurmanov S, Hojamberdiev M et al (2014) Fabrication of nitrogen-doped TiO_2 monolith with well-defined macroporous and bicrystalline framework and its photocatalytic performance under visible light. J Eur Ceram Soc 34:809–816. doi:10.1016/j.jeurceramsoc.2013.10.009
12. Khan W, Ahmad S, Naqvi AH (2014) Formation of self-assembled spherical-flower like nanostructures of cobalt doped anatase TiO_2 and its optical band-gap. Mater Lett 133:28–31. doi:10.1016/j.matlet.2014.06.121
13. Peng Ruan, Jieshu Qian, Yifan Xu, Haixian Xie CS and XZ (2013) Mixed-phase TiO_2 nanorods assembled microsphere: crystal phase control and photovoltaic application 3. 5093–5099. doi: 10.1039/c3ce40351c
14. Schütz C, Sort J, Bacsik Z et al (2012) Hard and transparent films formed by nanocellulose–TiO_2 nanoparticle hybrids. PLoS One 7:e45828. doi:10.1371/journal.pone.0045828
15. Ananpattarachai J, Kajitvichyanukul P, Seraphin S (2009) Visible light absorption ability and photocatalytic oxidation activity of various interstitial N-doped TiO_2 prepared from different nitrogen dopants. J Hazard Mater 168:253–261. doi:10.1016/j.jhazmat.2009.02.036
16. Moharram AH, Mansour SA, Hussein MA, Rashad M (2014) Direct precipitation and characterization of ZnO Nanoparticles. J Nanomater 2014:1–5. doi:10.1155/2014/716210
17. Zhang YC, Yang M, Zhang G, Dionysiou DD (2013) HNO_3^- involved one-step low temperature solvothermal synthesis of N-doped TiO_2 nanocrystals for efficient photocatalytic reduction of Cr(VI) in water. Appl Catal B Environ 142–143:249–258. doi:10.1016/j.apcatb.2013.05.023
18. Dong F, Guo S, Wang H et al (2011) Enhancement of the visible light photocatalytic activity of C-doped TiO_2 nanomaterials prepared by a green synthetic approach. J Phys Chem C 115:13285–13292

19. Selvaraj A, Parimiladevi R, Rajesh KB (2013) Synthesis of nitrogen doped titanium dioxide (TiO_2) and its photocatalytic performance for the degradation of indigo carmine dye. J Environ Nanotechnol 2:28–31. doi:10.13074/jent.2013.02.121026
20. Chen Q, Liu H, Xin Y, Cheng X (2013) TiO_2 nanobelts—effect of calcination temperature on optical, photoelectrochemical and photocatalytic properties. Electrochim Acta 111:284–291. doi:10.1016/j.electacta.2013.08.049
21. Hu L, Wang J, Zhang J et al (2014) An N-doped anatase/rutile TiO_2 hybrid from low-temperature direct nitridization: enhanced photoactivity under UV–/visible-light. RSC Adv 4:420. doi:10.1039/c3ra44421j
22. Qiao M, Chen Q, Wu S, Shen J (2010) Novel sol–gel synthesis of N-doped TiO_2 hollow spheres with high photocatalytic activity under visible light. J Sol–gel Sci Technol 55:377–384. doi:10.1007/s10971-010-2253-2
23. Wang Q, Jiang Z, Wang Y et al (2008) Photocatalytic properties of porous C-doped TiO_2 and Ag/C-doped TiO_2 nanomaterials by eggshell membrane templating. J Nanoparticle Res 11:375–384. doi:10.1007/s11051-008-9390-3
24. Gamage McEvoy J, Cui W, Zhang Z (2013) Degradative and disinfective properties of carbon-doped anatase–rutile TiO_2 mixtures under visible light irradiation. Catal Today 207:191–199. doi:10.1016/j.cattod.2012.04.015
25. Xing M, Li X, Zhang J (2014) Synergistic effect on the visible light activity of Ti_3^+ doped TiO_2 nanorods/boron doped graphene composite. Sci Rep 4:5493. doi:10.1038/srep05493
26. Liu H, Imanishi A, Nakato Y (2007) Mechanisms for photooxidation reactions of water and organic compounds on carbon-doped titanium dioxide, as studied by photocurrent measurements. J Phys Chem C 111:8603–8610. doi:10.1021/jp070771q
27. Irie H, Watanabe Y, Hashimoto K (2003) Carbon-doped anatase TiO_2 powders as a visible-light sensitive photocatalyst. Chem Lett 32:772–773. doi:10.1246/cl.2003.772
28. Choi Y (2004) Fabrication and characterization of C-doped anatase TiO_2 photocatalysts. J Mater Sci 39:1837–1839
29. Fang J, Wang F, Qian K et al (2008) Bifunctional N-doped mesoporous TiO_2 photocatalysts. J Phys Chem C 112:18150–18156. doi:10.1021/jp805926b
30. Xu J, Wang F, Liu W, Cao W (2013) Nanocrystalline N-doped TiO_2 powders : mild hydrothermal synthesis and photocatalytic degradation of phenol under visible light irradiation. Int J Photoenergy 2013:1–7
31. Wang Z, Cai W, Hong X et al (2005) Photocatalytic degradation of phenol in aqueous nitrogen-doped TiO_2 suspensions with various light sources. Appl Catal B Environ 57:223–231. doi:10.1016/j.apcatb.2004.11.008
32. Yates HM, Nolan MG, Sheel DW, Pemble ME (2006) The role of nitrogen doping on the development of visible light-induced photocatalytic activity in thin TiO_2 films grown on glass by chemical vapour deposition. J Photochem Photobiol A Chem 179:213–223. doi:10.1016/j.jphotochem.2005.08.018
33. Zhu L, Xie J, Cui X et al (2010) Photoelectrochemical and optical properties of N-doped TiO_2 thin films prepared by oxidation of sputtered TiN_x films. Vacuum 84:797–802. doi:10.1016/j.vacuum.2009.10.040
34. Wang Y, Feng C, Jin Z et al (2006) A novel N-doped TiO_2 with high visible light photocatalytic activity. J Mol Catal A Chem 260:1–3. doi:10.1016/j.molcata.2006.06.044
35. Viswanathan B, Krishanmurthy KR (2012) Nitrogen incorporation in TiO_2: does it make a visible light photo-active material? Int J Photoenergy 2012:1–10. doi:10.1155/2012/269654
36. Yang G, Jiang Z, Shi H et al (2010) Preparation of highly visible-light active N-doped TiO_2 photocatalyst. J Mater Chem 20:5301. doi:10.1039/c0jm00376j
37. Peng F, Cai L, Yu H et al (2008) Synthesis and characterization of substitutional and interstitial nitrogen-doped titanium dioxides with visible light photocatalytic activity. J Solid State Chem 181:130–136. doi:10.1016/j.jssc.2007.11.012
38. Yang X, Cao C, Erickson L et al (2008) Synthesis of visible-light-active TiO_2^- based photocatalysts by carbon and nitrogen doping. J Catal 260:128–133. doi:10.1016/j.jcat.2008.09.016
39. Sayed F, Jayakumar O (2012) Photochemical hydrogen generation using nitrogen-doped TiO_2^- Pd nanoparticles: facile synthesis and effect of Ti_3^+ incorporation. J Phys Chem C 116:12462–12467
40. Zhang M, Lu D, Yan G et al (2013) Fabrication of Mo+ N-codoped TiO_2 nanotube arrays by anodization and sputtering for visible light-induced photoelectrochemical and photocatalytic properties. J Nanomater 2013:1–9
41. Wan L, Li JF, Feng JY et al (2007) Improved optical response and photocatalysis for N-doped titanium oxide (TiO_2) films prepared by oxidation of TiN. Appl Surf Sci 253:4764–4767. doi:10.1016/j.apsusc.2006.10.047
42. Zhang M, Wu J, Lu D, Yang J (2013) Enhanced visible light photocatalytic activity for TiO_2 nanotube array films by codoping with tungsten and nitrogen. Int J Photoenergy 2013:1–8
43. Yang K, Dai Y, Huang B (2007) Study of the nitrogen concentration influence on N-doped TiO_2 anatase from first-principles calculations. J Phys Chem C 111:12086–12090
44. Higashimoto S, Takamatsu K, Azuma M et al (2007) Enhancement of the photocatalytic activity under visible-light irradiation over N-doped TiO_2 modified by platinum chloride. Catal Lett 122:33–36. doi:10.1007/s10562-007-9333-0
45. Dang M, Zhou Y, Li H, Lv C (2011) Preparation and photocatalytic activity of N-doped TiO_2 nanotube array films. J Mater Sci Mater Electron 23:320–324. doi:10.1007/s10854-011-0413-y
46. Mothi KM, Soumya G, Salim AH, Sugunan S (2014) Visible light active Ag, N co-doped titania in the photo-oxidation of some 9-(*N*, *N*-dimethylaminomethyl) anthracene systems. J Sol–gel Sci Technol 71:549–556. doi:10.1007/s10971-014-3389-2
47. Lin X, Rong F, Ji X, Fu D (2011) Visible light photocatalytic activity and photoelectrochemical property of Fe-doped TiO_2 hollow spheres by sol–gel method. J Sol–gel Sci Technol 59:283–289. doi:10.1007/s10971-011-2497-5